arXiv:1107.1443v1 [physics.chem-ph] 7 Jul 2011

Cold collisions of an open-shell S-state atom with a $^2\Pi$ molecule: N(^{4}S) colliding with OH in a magnetic field

Wojciech Skomorowski,[a] **Maykel L. González-Martínez,**[b] **Robert Moszynski,***[a] **and Jeremy M. Hutson***[b]

We present quantum-theoretical studies of collisions between an open-shell S-state atom and a $^2\Pi$-state molecule in the presence of a magnetic field. We analyze the collisional Hamiltonian and discuss possible mechanisms for inelastic collisions in such systems. The theory is applied to the collisions of the nitrogen atom (^{4}S) with the OH molecule, with both collision partners initially in fully spin-stretched (magnetically trappable) states, assuming that the interaction takes place exclusively on the two high-spin (quintet) potential energy surfaces. The surfaces for the quintet states are obtained from spin-unrestricted coupled-cluster calculations with single, double, and noniterative triple excitations. We find substantial inelasticity, arising from strong couplings due to the anisotropy of the interaction potential and the anisotropic spin-spin dipolar interaction. The mechanism involving the dipolar interaction dominates for small magnetic field strengths and ultralow collision energies, while the mechanism involving the potential anisotropy prevails when the field strength is larger (above 100 G) or the collision energy is higher (above 1 mK). The numerical results suggest that sympathetic cooling of magnetically trapped OH by collisions with ultracold N atoms will not be successful at higher temperatures.

1 Introduction

The first experimental realization of Bose-Einstein condensation in a dilute gas in 1995[1] opened up a novel and fast-growing field of research on cold and ultracold matter. At temperatures below about 10^{-6} K, novel properties emerge in which the quantum nature of atoms and molecules is crucial. Although the original experiments involved quantum-degenerate states in atomic systems, it was soon realised that molecules, especially those with a permanent dipole moment, offer an additional range of applications in physics and chemistry. These include development of new frequency standards, tests of fundamental physical concepts such as parity and time-reversal violation[2,3], spectroscopic measurements of unprecedented accuracy[4,5], quantum information processing,[6,7], and control of chemical reactions with state-selected reagents and products[8–10].

In contrast to atoms, which nowadays can be cooled relatively easily by laser Doppler cooling and evaporative cooling[11], molecules are incomparably more challenging because of their complicated internal structure. Two main classes of methods have been established to produce cold molecules: direct methods, in which molecules are cooled from high temperature by means of a buffer gas or external fields, and indirect methods, in which cold molecules are formed from precooled atoms by photoassociation or magnetoassociation.

Indirect methods can now produce ground-state molecules at temperatures below 1 μK[12–14]. It has been shown recently that, for KRb, the rates of chemical reactions change spectacularly between different nuclear spin states and can be dramatically affected by applied electric fields[10]. However, indirect methods are so far restricted to alkali-metal dimers and it will be challenging to extend them to other regions of the periodic table[15].

Direct cooling methods can be applied to a much larger variety of chemically interesting molecules, including OH, NH_3, CO and LiH[16–19]. Stark deceleration, pioneered by Meijer and coworkers[16], can be applied to polar molecules with large Stark effects, while helium buffer-gas cooling[20] has been particularly successful for paramagnetic species. However, the temperatures so far achieved with direct methods are limited to tens of millikelvin, which is not cold enough to achieve quantum degeneracy. The development of a second-stage cooling method for such molecules is the biggest current challenge in the field. One of the most promising proposals is to use *sympathetic cooling*, which is based on the conceptually simple idea of bringing cold molecules into thermal contact with a bath containing ultracold atoms. So far sympathetic cooling has been successfully realized for ions[21,22] and some neutral atoms[23,24], but not for neutral molecules.

Linear molecules in spatially degenerate electronic states (Π, Δ, etc.) are particularly attractive for Stark deceleration, as they exhibit first-order Stark effects at moderate electric fields (in contrast to molecules in Σ states, which exhibit only second-order Stark effects). After deceleration, the molecules

[a] *Faculty of Chemistry, University of Warsaw, Pasteura 1, 02-093 Warsaw, Poland. E-mail: rmoszyns@tiger.chem.uw.edu.pl*
[b] *Department of Chemistry, Durham University, South Road, Durham DH1 3LE, United Kingdom. E-mail:J.M.Hutson@durham.ac.uk*

can be loaded into traps where they are confined by static electric or magnetic fields. Such static traps are not the only way to confine cold molecular species[25], but they are experimentally the most accessible. In addition, atoms in open-shell S states (such as alkali-metal atoms, H(^{2}S), N(^{4}S), He(^{3}S), and Cr(^{7}S)), can be held in magnetic traps and may be suitable as coolants.

Trapping with a static field is possible only if the atom or molecule is in a low-field-seeking state. However, the absolute ground state is always high-field-seeking. Thus, in addition to the elastic collisions that lead to thermalization of the sample, there is always the possibility of inelastic collisions that transfer the colliding partners to a lower state and release kinetic energy. Inelastic collisions eject molecules from the trap and may lead to the heating of the sample. The success of sympathetic cooling therefore depends on the ratio of elastic to inelastic events, which should preferably be as large as possible.

Molecular sympathetic cooling was first suggested for Rb+NH($^3\Sigma^-$)[26]. Subsequently, potential energy surfaces and the appropriate collision cross sections have been calculated for a variety of candidate systems, including Mg+NH($^3\Sigma^-$)[27], Li+LiH($^1\Sigma^+$)[28,29], Rb+NH_3[30] and He+CH_2($^3B_1$)[31]. Rb+ND_3 has also been explored experimentally[32], though the inelastic collision rate in an electric field turned out to be too high for cooling. Studies of cold collisions with linear molecules in a Π state in the presence of external fields have mostly been limited to cases when the second colliding partner is closed-shell. In particular, Tscherbul *et al.*[33] have investigated OH+He collisions and have shown how the inelastic cross sections can be reduced by combining electric and magnetic fields to eliminate certain inelastic channels. Collisions of rotationally excited OH with He in the presence of electromagnetic field were analyzed by Pavlovic *et al.*[34], while Bohn and coworkers[35] studied cold collisions between two OH molecules with long-range dipole-dipole interactions and concluded that the evaporative cooling of OH would be challenging. Lara *et al.*[36] carried out theoretical studies of cold collisions of OH with Rb, taking account of multiple potential energy surfaces and including the hyperfine structure of OH. However, they did not include external field effects.

There is thus a need for rigorous quantum studies of collisions between a Π-state molecule and an open-shell S-state atom in the presence of external fields. In this paper, we extend the theory presented in Refs.[36,37] to handle this case. This theory will be applicable to a broad set of experimentally important systems, including interactions of molecules such as OH, NO, ClO, and CH with alkali-metal and other magnetically trappable atoms. As an example, we present numerical results for collisions between OH($^2\Pi$) and N(^{4}S) in a magnetic field, with both colliding species initially in their fully spin-stretched low-field-seeking states. OH was one of the first molecules to be decelerated and trapped[19,38], and many pioneering experiments with it have been reported. Gilijamse *et al.*[19] carried out a crossed-beam experiment, colliding velocity-controlled OH molecules with Xe atoms; they were able to resolve state-to-state inelastic cross sections as a function of the collision energy. Similar experiments with improved sensitivity have recently been performed for OH colliding with Ar, He, and D_2[39–41]. An experiment to collide two velocity-controlled beams, of OH and NO, is in preparation[42]. Sawyer *et al.*[38] have measured energy-dependent cross sections for collisions between magnetically trapped OH and slow D_2 molecules.

Tscherbul *et al.*[43] have recently suggested that spin-polarized nitrogen atoms are a promising coolant for sympathetic cooling experiments. N atoms at $T > 1$ mK are stable against collisional relaxation between different Zeeman levels for a wide range of magnetic field strengths. Moreover, the low polarizability of the N atom leads to potential energy surfaces with an anisotropy much smaller than is usually encountered for interactions with alkali-metal atoms. Theoretical and experimental studies for collisions of magnetically trapped N(^{4}S) and NH($^3\Sigma^-$) have been reported[44,45], showing that the trap loss in this system is fairly small and is caused mostly by the anisotropic magnetic dipole-dipole interaction between the atomic and molecular spins.

This paper is organized as follows. In Sec. II we describe calculations of the high-spin (quintet) potential energy surfaces resulting from interaction of the N(^{4}S) atom with the OH($^2\Pi$) molecule. In Sec. III we describe the effective Hamiltonian used in the dynamical calculations and give the expressions for the matrix elements of the Hamiltonian. In Sec. IV we discuss the results of the scattering calculations and their implications for sympathetic cooling of OH by N atoms. Finally, Sec. V summarizes and concludes the paper.

2 Potential energy surfaces

The interaction between the N(^{4}S) atom and the OH($^2\Pi$) molecule occurs on four adiabatic surfaces: $^3A'$, $^3A''$, $^5A'$, and $^5A''$. The triplet surfaces have been studied extensively to investigate the reaction N+OH→NO+H that can take place on the $^3A''$ surface[46–51]. This reaction is the major source of the NO radical in the interstellar medium and is one of the key elementary processes in nitrogen chemistry. Formation of NO is barrierless, via a stable intermediate complex NOH, and is highly exothermic with 1.83 eV energy release. The other possible reaction channel N+OH→NH+O is energetically forbidden for low-energy collisions. If we neglect minor spin-orbit coupling effects between the triplet and quintet states, the quintet surfaces are non-reactive. To our knowledge, the

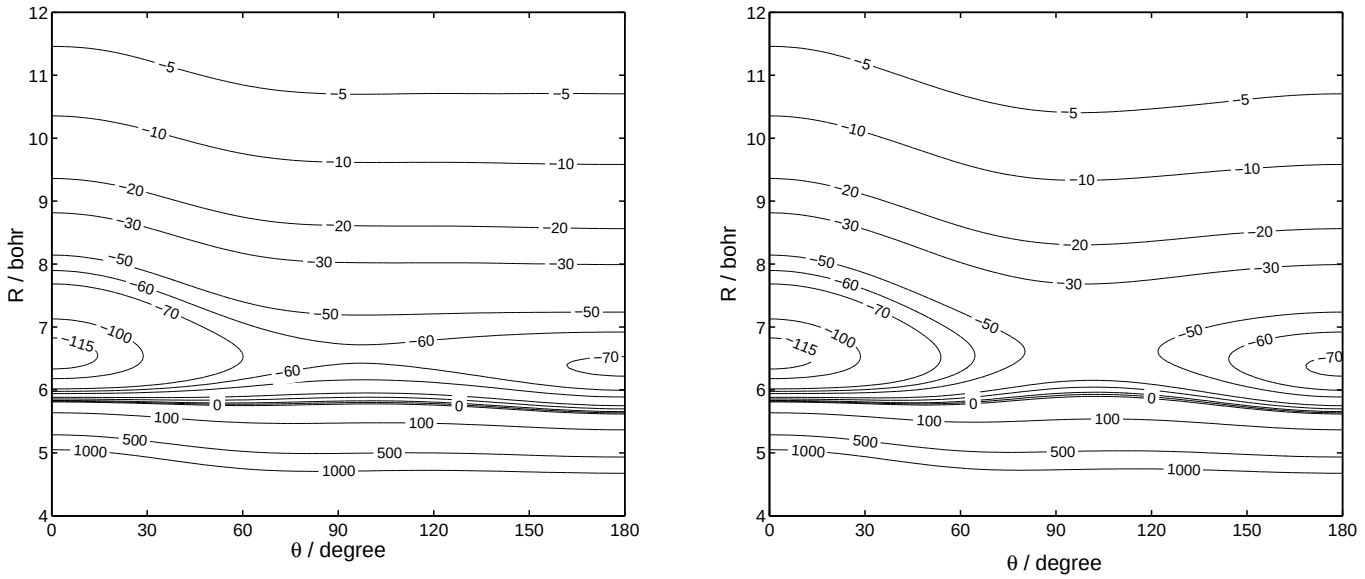

Fig. 1 Contour plots of the quintet interaction potentials for N+OH: $^5A'$ (left-hand panel) and $^5A''$ (right-hand panel). Energies are in cm^{-1}.

quintet surfaces of N+OH have not been reported in the literature thus far.

We have carried out calculations of the quintet surfaces using the unrestricted version of the coupled-cluster method with single, double, and noniterative triple excitations [UCCSD(T)]. The unrestricted version was chosen to circumvent the problem of the lack of size-consistency for the interaction between two open-shell systems in spin-restricted coupled-cluster calculations[52]. The highly accurate aug-cc-pV5Z basis set of Dunning[53] was employed for all atoms and the counterpoise procedure[54] was used to correct the computed interaction energies for basis-set superposition error. The MOLPRO suite of codes[55] was used in the electronic structure calculations.

Both the $^5A'$ and $^5A''$ potential energy surfaces were computed on a grid of points in Jacobi coordinates (R, θ), where R is the intermolecular distance measured from the centre of mass of ^{16}OH to the ^{14}N atom and θ is the angle between the vector pointing from O to H in the OH molecule and the vector pointing from the centre of mass of OH to the N atom. The angle $\theta = 0°$ thus corresponds to the linear O–H—N arrangement. The distance R was varied from 4.0 to 12.0 a_0 with an interval of 0.5 a_0 and from 12.0 to 20.0 a_0 with an interval of 1.0 a_0. The angular grid points was chosen as the set of points for 11-point Gauss-Lobatto quadrature, which include points at $\theta = 0$ and 180°. The OH bond length was kept fixed at the monomer equilibrium value of 1.834 a_0.

Table 1 Characteristic points of the interaction potentials for the quintet states of N(^{4}S) + OH($^2\Pi$).

	R / a_0	θ / degrees	V / cm^{-1}	Surface
Global minimum	6.55	0.0°	–120.9	$^5A'$, $^5A''$
Local minimum	6.36	180.0°	–71.5	$^5A'$, $^5A''$
Saddle point	6.56	97.2°	–61.0	$^5A'$
Saddle point	6.66	100.1°	–45.8	$^5A''$

Contour plots of the $^5A'$ and $^5A''$ potential energy surfaces are shown in Fig. 1. The shapes of the two quintet potentials are quite similar. The global minima appear for the linear geometry O–H—N and have a depth of 120.9 cm^{-1}. There are also local minima 71.5 cm^{-1} deep, which occur at the linear N—O–H configuration. Note that for linear geometries the $^5A'$ and $^5A''$ states are degenerate, so these minima are common to the two surfaces. The set of stationary points of the potentials is completed by saddle points between the two minima, which are located at slightly different positions for the $^5A'$ and $^5A''$ states. Table 1 gives the positions of the stationary points on the surfaces and the corresponding interaction energies. The shapes of the quintet potential energy surfaces for N+OH closely resemble the high-spin (quartet) surface for N+NH reported by Żuchowski and Hutson[44], although the global minimum for N+OH is about 30 cm^{-1} deeper than for N+NH.

To perform quantum scattering calculations, it is necessary to expand the $^5A'$ and $^5A''$ surfaces in terms of angular functions. We adopt the convention of Alexander[37] and use spherical harmonics in the Racah normalization $C_{k,q}(\theta, \phi)$ (with an-

gle $\phi = 0$) for angular representation of the potential. For the interaction of an S-state atom with a Π-state molecule, there are nonvanishing terms with $q = 0$ and $q = 2$. The sum of the $^5A'$ and $^5A''$ potentials is expanded in terms of functions with $k = 0$,

$$\frac{1}{2}\left[V_{A'}(R,\theta) + V_{A''}(R,\theta)\right] = \sum_{k=0}^{\infty} C_{k,0}(\theta,0) V_{k0}(R), \quad (1)$$

while the difference between the $^5A'$ and $^5A''$ potentials is expanded in terms of functions with $k = 2$,

$$\frac{1}{2}\left[V_{A'}(R,\theta) - V_{A''}(R,\theta)\right] = \sum_{k=2}^{\infty} C_{k,2}(\theta,0) V_{k2}(R). \quad (2)$$

Note that the definition of the difference potential, either $V_{A'} - V_{A''}$ or $V_{A''} - V_{A'}$, depends in general on the symmetry of the electronic wave functions of the interacting subsystems[56,57]. The radial functions $V_{kq}(R)$ are obtained by projecting the sum or difference onto the appropriate angular function, using Gauss-Lobatto quadrature to perform the numerical integration. Prior to this projection, the interpolation to obtain $V_{A'}(R,\theta)$ and $V_{A''}(R,\theta)$ at an arbitrary value of R is done for each value of θ using the reproducing kernel Hilbert space (RKHS) procedure[58]. For the quintet states of N(^{4}S)+OH(^{2}Π), the dominant anisotropic term in the expansion (1) is $V_{20}(R)$ with a well depth of approximately 28 cm^{-1}, while the dominant term in the expansion (2) comes from $V_{22}(R)$.

To improve the description of the potential at large R, we use an analytic representation in this region. Each radial component $V_{kq}(R)$ is expanded at long range in terms of Van der Waals coefficients,

$$V_{kq}(R) = -\sum_{n=6} C_n^{kq}/R^n. \quad (3)$$

The expressions for the C_n^{kq} coefficients have been given by Skomorowski and Moszynski[57], though with a different normalisation for $q > 0$ from the one used here. We calculated the Van der Waals constants up to and including n=8, using the method described in Ref.[57]. The results are listed in Table 2. For a weakly polarizable system such as N+OH, the neglect of higher-order coefficients with $n > 8$ is fully justified. We used the switching function of Janssen *et al.*[52], with parameters $a = 15\ a_0$ and $b = 25\ a_0$, to join the asymptotic form based on the long-range coefficients and the RKHS interpolation of the *ab initio* points.

Table 2 Long-range coefficients (in atomic units) for N(^{4}S)+OH(^{2}Π).

$k \rightarrow$	0	1	2	3	4
C_6^{k0}	27.84		4.92		
C_6^{k2}			1.23		
C_7^{k0}		51.60		24.61	
C_7^{k2}				–6.38	
C_8^{k0}	583.34		312.00		48.29
C_8^{k2}			159.09		31.42

3 Collision Hamiltonian

3.1 Effective Hamiltonian

We consider the case of an atom A($^{2s_1+1}$S), interacting with a diatomic molecule BC(^{2}Π), in the presence of an external magnetic field B. The direction of the field defines the laboratory (space-fixed) Z-axis. The system A–BC is described in Jacobi coordinates, with the $\boldsymbol{r}$ vector connecting the heavier and lighter of the atoms B and C, and $\boldsymbol{R}$ connecting the centre of mass of BC and the atom A. By convention, lower-case and capital letters are used to represent the quantum numbers of the monomers and of the complex as a whole, respectively. The subscripts 1 and 2 refer to the monomers A and BC, respectively. For simplicity, the diatom will be treated as a rigid rotor in vibrational state v, although generalization to include its vibrations is straightforward.

The Hamiltonian describing the nuclear motions of A+BC in the presence of magnetic field B can be written

$$\hat{H} = -\frac{\hbar^2}{2\mu} R^{-1} \frac{d^2}{dR^2} R + \frac{\hat{L}^2}{2\mu R^2} + \hat{H}_{\rm mon} + \hat{H}_{12}, \quad (4)$$

where $\hat{L}$ is the space-fixed angular momentum operator describing the end-over-end rotation of A and BC about one another and μ is the reduced mass of the complex. $\hat{H}_{\rm mon}$ contains all terms describing the *isolated* monomers, i.e. $\hat{H}_{\rm mon} = \hat{H}_1 + \hat{H}_2$. $\hat{H}_{12}$ describes the interaction between the monomers:

$$\hat{H}_{12} = \hat{H}_{\rm s_1 s_2} + \hat{V}(R,\theta). \quad (5)$$

Here, $\hat{H}_{\rm s_1 s_2}$ accounts for the direct dipolar interaction between the magnetic moments due to the unpaired electrons of the monomers, and $\hat{V}$ is the intermolecular interaction potential.

If $s_1 \neq 0$ and hyperfine terms are neglected, the Hamiltonian for an isolated atom in the state $^{2s_1+1}$S is fully determined by the Zeeman interaction between the electron spin and the external magnetic field,

$$\hat{H}_1 = g_S \mu_{\rm B}\ \hat{s}_1 \cdot \hat{B}, \quad (6)$$

where g_S is the electron g-factor, $\mu_{\rm B}$ is the electron Bohr magneton, and $\hat{s}_1$ is the spin operator.

The analogous Hamiltonian for a ^{2}Π molecule can be written[59]

$$\hat{H}_2 = \hat{H}_{\rm rso} + \hat{H}_{{\rm Z},2} + \hat{H}_{\lambda}, \quad (7)$$

where the rotational and spin-orbit contributions within the Π state are collapsed into the first term,

$$\hat{H}_{\rm rso} \equiv B_v\,\hat{n}^2 + A_v\,\hat{l}\cdot\hat{s_2}. \quad (8)$$

B_v and A_v are the molecular rotational and spin-orbit constants, respectively, and $\hat{n}$ is the operator of the mechanical rotation of BC, which can be expressed as $\hat{j}-\hat{l}-\hat{s}_2$, where $\hat{j}$, $\hat{l}$ and $\hat{s}_2$ are the operators for the rotational, electronic orbital and spin angular momenta, respectively. $\hat{H}_{\rm rso}$ can be rewritten

$$\begin{aligned}\hat{H}_{\rm rso} &= (A_v+2B_v)\,\hat{l}_z\hat{s}_{2z} \\ &\quad +B_v\Big[\hat{j}^2+\hat{l}^2+\hat{s}_2^2-2\hat{j}\cdot\hat{s}_2+\hat{l}_z^2-2\hat{j}_z\,\hat{l}_z\Big]. \quad (9)\end{aligned}$$

The terms $\hat{l}^2$, $\hat{s}_2^2$ and $\hat{l}_z^2$ simply shift all the levels by a constant amount and are omitted below. The term $\hat{H}_\lambda$, responsible for the Λ-doubling of the rotational levels of BC, is represented by the effective Hamiltonian

$$\hat{H}_\lambda = \sum_{q=\pm1} {\rm e}^{-2{\rm i}q\phi_r}\left[-q_v{\rm T}^2_{2q}(\hat{j},\hat{j})+(p_v+2q_v){\rm T}^2_{2q}(\hat{j},\hat{s}_2)\right], \quad (10)$$

where ϕ_r is the azimuthal angle associated with the electron orbital angular momentum about the molecular axis defined by $\boldsymbol{r}$, while p_v and q_v are empirical parameters. In Eq. (10), the second-rank tensor ${\rm T}^2_q$ that couples two vectors $\mathbf{k}_1$ and $\mathbf{k}_2$ is defined as

$${\rm T}^2_q(\mathbf{k}_1,\mathbf{k}_2) = \sum_{q_1,q_2}\langle 1,q_1;1,q_2|2,q\rangle {\rm T}^1_{q_1}(\mathbf{k}_1)\,{\rm T}^1_{q_2}(\mathbf{k}_2), \quad (11)$$

where $\langle 1,q_1;1,q_2|2,q\rangle$ is a Clebsch-Gordan coefficient and the first-rank tensor components are ${\rm T}^1_0(\mathbf{k}) = {\rm k}_z$ and ${\rm T}^1_{\pm1}(\mathbf{k}) = \mp({\rm k}_x \pm i\,{\rm k}_y)/\sqrt{2}$. If only the electron spin and orbital contributions are taken into account, the Zeeman term is

$$\hat{H}_{\rm Z,2} = g_S\mu_{\rm B}\,\hat{s}_2\cdot\hat{B} + g'_L\mu_{\rm B}\,\hat{l}\cdot\hat{B}, \quad (12)$$

where g'_L is the orbital g-factor. For diatomic molecules of multiplicity higher than 2 (for example $^3\Pi$), an additional term describing the intramolecular spin-spin interaction must be included in the monomer Hamiltonian (7).

The spin-spin dipolar interaction can conveniently be written[59]:

$$\hat{H}_{\rm s_1s_2} = -g_S^2\mu_B^2(\mu_0/4\pi)\sqrt{6}\sum_q(-1)^q\,{\rm T}^2_q(\hat{s}_1,\hat{s}_2)\,{\rm T}^2_{-q}(\boldsymbol{C}), \quad (13)$$

with ${\rm T}^2_q(\boldsymbol{C}) = C_{2,q}(\theta,\phi)R^{-3}$, where $C_{2,q}(\theta,\phi)$ is a spherical harmonic function in the Racah normalization and (R,θ,ϕ) is the set of relative spherical coordinates of the 'composite' atomic and diatomic electronic spins in the space-fixed frame. μ_0 is the magnetic permeability of the vacuum.

3.2 Basis sets and matrix elements

The state of the BC molecule can conveniently be described using Hund's case (a) basis functions $|\lambda;s_2\sigma_2;j\omega m_j\rangle$, where s_2 is the electron spin with projection σ_2 onto the molecular axis (body-fixed z axis), λ is the (signed) projection of the electronic orbital angular momentum onto the molecular axis, and j is the angular momentum of BC with projections ω onto the molecular axis and m_j onto the space-fixed Z-axis. For the body-fixed projections we have $\omega = \lambda+\sigma$. The state of the atom is characterized by the electronic spin function $|s_1 m_{s_1}\rangle$. The basis set used here for the A–BC collision system is constructed as $|s_1 m_{s_1}\rangle\,|\lambda;s_2\sigma_2;j\omega m_j\rangle\,|LM_L\rangle$, where $|LM_L\rangle$ are functions describing the relative motion of A and BC in the space-fixed reference frame.

In the presence of a magnetic field, the conserved quantities are the projection $M_{\rm tot}$ of the total angular momentum, $M_{\rm tot} = m_{s_1}+m_j+M_L$, and the total parity $\mathcal{P}$. An electric field would mix states of different total parity. In the absence of an electric field it is most efficient to use a parity-adapted basis set, $|s_1 m_{s_1}\rangle\,|s_2;j\bar{\omega}m_j\epsilon\rangle\,|LM_L\rangle$, with

$$\begin{aligned}|s_2;j\bar{\omega}m_j\epsilon\rangle \equiv &\frac{1}{\sqrt{2}}\Big[\,|1;s_2\sigma_2;j\bar{\omega}m_j\rangle \\ &+\epsilon(-1)^{j-s_2}\,|-1;s_2\,-\sigma_2;j\,-\bar{\omega}m_j\rangle\Big],\end{aligned} \quad (14)$$

where $\bar{\omega}\equiv|\omega|$, $\sigma_2 = \bar{\omega}-1$ and $\epsilon = \pm1$. In this basis set, the parity of BC is $p_2 = \epsilon(-1)^{j-s_2}$, and that of the triatomic system is $\mathcal{P} = p_1p_2(-1)^L$. The matrix elements of $\hat{L}^2$ and $\hat{H}_1$ are diagonal, and given by $\hbar^2L(L+1)$ and $g_S\mu_{\rm B}m_{s_1}B$, respectively.

We next give the matrix elements of all terms in the Hamiltonian of Eq. (4), although only those involving the atomic spin are new in the present work. The terms that do not involve atomic spin are the same as for collisions with a closed-shell atom and were previously given by Tscherbul *et al.*[33]. However, the published version of Ref.[33] contains a number of typographical errors, so we report the correct expressions here.

The matrix elements of the molecular rotation/spin-orbit operator are

$$\begin{aligned}&\langle s_2;j\bar{\omega}m_j\epsilon|\,\hat{H}_{\rm rso}\,|s_2;j\bar{\omega}'m_j\epsilon\rangle \\ &\quad=\delta_{\bar{\omega}\bar{\omega}'}\Big\{(A_v+2B_v)(\bar{\omega}-1)+B_v\left[j(j+1)-2\bar{\omega}^2\right]\Big\} \\ &\qquad -B_v\Big[\delta_{\bar{\omega}\bar{\omega}'-1}\alpha_-(j,\bar{\omega}')\alpha_-(s_2,\bar{\omega}'-1) \\ &\qquad\quad +\delta_{\bar{\omega}\bar{\omega}'+1}\alpha_+(j,\bar{\omega}')\alpha_+(s_2,\bar{\omega}'-1)\Big], \end{aligned} \quad (15)$$

where we use $\alpha_\pm(j,m)\equiv\sqrt{j(j+1)-m(m\pm1)}$ both to simplify the equations and to ease comparison with Ref.[33]. The off-diagonal terms on the right-hand side connect different spin-orbit manifolds related by $\bar{\omega}' = \bar{\omega}\pm1$.

The Λ-doubling matrix elements are

$$\langle s_2; j\bar{\omega} m_j \epsilon | \hat{H}_\lambda | s_2; j\bar{\omega}' m_j \epsilon \rangle = \frac{1}{2}\epsilon(-1)^{j-s_2}\alpha_-(j,\bar{\omega}') \times \left[\delta_{\bar{\omega}2-\bar{\omega}'} q_v \alpha_-(j,\bar{\omega}'-1) - \delta_{\bar{\omega}1-\bar{\omega}'}(p_v+2q_v)\alpha_+(s_2,\bar{\omega}'-1)\right] \quad (16)$$

and also couple states with different $\bar{\omega}$. For a $^2\Pi$ molecule, the first factor inside the square brackets mixes the $1/2$ and $3/2$ states, while the second is non-zero only for $\bar{\omega} = \bar{\omega}' = 1/2$.

The matrix elements of the Zeeman interaction for the molecule BC are

$$\begin{aligned}&\langle s_2; j\bar{\omega} m_j \epsilon | \hat{H}_{\mathrm{Z},2} | s_2; j'\bar{\omega}' m_j \epsilon \rangle \\ &= \mu_\mathrm{B} B (-1)^{m_j-\bar{\omega}'} \left[(2j+1)(2j'+1)\right]^{1/2} \begin{pmatrix} j & 1 & j' \\ m_j & 0 & -m_j \end{pmatrix} \\ &\times \left[g_S \frac{\alpha_+(s_2,\bar{\omega}'-1)}{\sqrt{2}} \begin{pmatrix} j & 1 & j' \\ \bar{\omega} & -1 & -\bar{\omega}' \end{pmatrix} - g_S \frac{\alpha_-(s_2,\bar{\omega}'-1)}{\sqrt{2}} \right. \\ &\left. \times \begin{pmatrix} j & 1 & j' \\ \bar{\omega} & 1 & -\bar{\omega}' \end{pmatrix} + \left[g_S(\bar{\omega}-1) + g'_L\right] \begin{pmatrix} j & 1 & j' \\ \bar{\omega} & 0 & -\bar{\omega}' \end{pmatrix} \right], \end{aligned} \quad (17)$$

and mix both different rotational and different spin-orbit states.

To determine the matrix elements of the spin-spin dipolar interaction it is natural to expand the second-rank tensor $\mathrm{T}^2(\hat{s}_1,\hat{s}_2)$ as a linear combination of the products of the space-fixed components of first-rank tensors $\mathrm{T}^1_{p_1}(\hat{s}_1)$ and $\mathrm{T}^1_{p_2}(\hat{s}_2)$. The matrix elements of $\mathrm{T}^1_{p_1}(\hat{s}_1)$ can be calculated directly in our basis set, while for $\mathrm{T}^1_{p_2}(\hat{s}_2)$ we first need to transform from the space- to the body-fixed frame,

$$\mathrm{T}^1_{p_2}(\hat{s}_2) = \sum_q \mathcal{D}^{(1)*}_{p_2 q}(\Omega)\mathrm{T}^1_q(\hat{s}_2), \quad (18)$$

where $\mathcal{D}^J_{KM}$ is a Wigner rotation matrix and Ω represents the Euler angles for the transformation. The matrix elements in the primitive basis set are

$$\begin{aligned}&\langle LM_L; \lambda; s_2\sigma_2; j\omega m_j; s_1 m_{s_1} | \hat{H}_{\mathrm{s_1 s_2}} | s_1 m'_{s_1}; \lambda; s_2\sigma'_2; j'\omega' m'_j; L' M'_L \rangle \\ &= -\sqrt{30}\lambda_{\mathrm{s_1 s_2}}(R)(-1)^{s_1-m_{s_1}+s_2-\sigma_2+m_j-\omega-M_L} \\ &\times \left[s_1(s_1+1)s_2(s_2+1)(2s_1+1)(2s_2+1)(2j+1)(2j'+1)\right]^{1/2} \\ &\times \left[(2L+1)(2L'+1)\right]^{1/2} \begin{pmatrix} L & 2 & L' \\ 0 & 0 & 0 \end{pmatrix} \\ &\times \sum_{p_1,p_2,q} \begin{pmatrix} 1 & 1 & 2 \\ p_1 & p_2 & -p \end{pmatrix} \begin{pmatrix} s_1 & 1 & s_1 \\ -m_{s_1} & p_1 & m'_{s_1} \end{pmatrix} \\ &\times \begin{pmatrix} s_2 & 1 & s_2 \\ -\sigma_2 & q & \sigma'_2 \end{pmatrix} \begin{pmatrix} j & 1 & j' \\ -m_j & p_2 & m'_j \end{pmatrix} \\ &\times \begin{pmatrix} j & 1 & j' \\ -\omega & q & \omega' \end{pmatrix} \begin{pmatrix} L & 2 & L' \\ -M_L & -p & M'_L \end{pmatrix}, \end{aligned} \quad (19)$$

and the corresponding matrix elements in the parity-adapted basis set are

$$\begin{aligned}&\langle LM_L; s_2; j\bar{\omega} m_j \epsilon; s_1 m_{s_1} | \hat{H}_{\mathrm{s_1 s_2}} | s_1 m'_{s_1}; s_2; j'\bar{\omega}' m'_j \epsilon; L' M'_L \rangle \\ &= \sqrt{30}\lambda_{\mathrm{s_1 s_2}}(R)(-1)^{s_1-m_{s_1}+s_2+m_j+2\bar{\omega}-M_L} \\ &\times \left[s_1(s_1+1)(2s_1+1)s_2(s_2+1)(2s_2+1)(2j+1)(2j'+1)\right]^{1/2} \\ &\times \left[(2L+1)(2L'+1)\right]^{1/2} \begin{pmatrix} L & 2 & L' \\ 0 & 0 & 0 \end{pmatrix} \\ &\times \sum_{p_1,p_2,q} \begin{pmatrix} 1 & 1 & 2 \\ p_1 & p_2 & -p \end{pmatrix} \begin{pmatrix} s_1 & 1 & s_1 \\ -m_{s_1} & p_1 & m'_{s_1} \end{pmatrix} \\ &\times \begin{pmatrix} s_2 & 1 & s_2 \\ -\bar{\omega}+1 & q & \bar{\omega}'-1 \end{pmatrix} \begin{pmatrix} j & 1 & j' \\ -m_j & p_2 & m'_j \end{pmatrix} \\ &\times \begin{pmatrix} j & 1 & j' \\ -\bar{\omega} & q & \bar{\omega}' \end{pmatrix} \begin{pmatrix} L & 2 & L' \\ -M_L & -p & M'_L \end{pmatrix}, \end{aligned} \quad (20)$$

where $p \equiv p_1 + p_2$, $\lambda_{\mathrm{s_1 s_2}}(R) = E_\mathrm{h} a_0^3 \alpha^2 / R^3$ is the R-dependent spin-spin dipolar coupling constant and $\alpha \approx 1/137$ is the fine-structure constant.

Finally, the matrix elements of the interaction potential are

$$\begin{aligned}&\langle LM_L; s_2; j\bar{\omega} m_j \epsilon | \hat{V} | s_2; j'\bar{\omega}' m'_j \epsilon'; L' M'_L \rangle \\ &= (-1)^{m_j-\bar{\omega}'-M_L} \left[(2j+1)(2j'+1)(2L+1)(2L'+1)\right]^{1/2} \\ &\times \sum_{k,m_k} \frac{1}{2}\left[1+\epsilon\epsilon'(-1)^k\right](-1)^{m_k} \begin{pmatrix} j & k & j' \\ m_j & m_k & -m'_j \end{pmatrix} \\ &\times \begin{pmatrix} L & k & L' \\ 0 & 0 & 0 \end{pmatrix} \begin{pmatrix} L & k & L' \\ -M_L & m_k & M'_L \end{pmatrix} \\ &\times \left[\begin{pmatrix} j & k & j' \\ \bar{\omega} & 0 & -\bar{\omega}' \end{pmatrix} V_{k0}(R) \right. \\ &\left. - (1-\delta_{\bar{\omega}\bar{\omega}'})\epsilon' \begin{pmatrix} j & k & j' \\ \bar{\omega} & -2 & \bar{\omega}' \end{pmatrix} V_{k2}(R) \right], \end{aligned} \quad (21)$$

where $V_{k0}(R)$ and $V_{k2}(R)$ are the radial strength functions of Eqs. (1) and (2). It is readily seen that states belonging to the same spin-orbit manifold are coupled through the 'average' of the A' and A'' potential surfaces, while those of different manifolds are connected through their difference. In addition, the factor $\frac{1}{2}\left[1+\epsilon\epsilon'(-1)^k\right]$ guarantees that states of the *same* monomer parity are connected by terms $V_{kq}(R)$ with *even* k, while those with *odd* k couple rotational levels of *opposite* parity. It follows from this that a strong parity-conserving propensity rule for transitions involving different spin-orbit manifolds can be expected.

4 Dynamical calculations

4.1 Computational details

Expanding the Schrödinger equation with the Hamiltonian of Eq. (4) in the parity-adapted basis set (14) yields a set of coupled differential equations. We have written a plug-in for the MOLSCAT general-purpose quantum molecular scattering package[60] to implement the matrix elements described above for collisions between an open-shell S-state atom and a $^2\Pi$-state molecule in a magnetic field. We solved the coupled equations numerically using the hybrid propagator of Alexander and Manolopoulos[61], propagating from $R_{\rm min} = 4\ a_0$ to $R_{\rm mid} = 25\ a_0$ using a fixed-step log-derivative propagator with interval size 0.02 a_0 and from $R_{\rm mid}$ to $R_{\rm max} = 800\ a_0$ using a variable-step log-derivative propagator based on Airy functions. MOLSCAT applies scattering boundary conditions at $R_{\rm max}$ to extract scattering S-matrices, which are then used to calculate elastic and inelastic cross sections.

Values of the OH molecular constants in the monomer Hamiltonian were taken from Refs.[62,63]. After performing numerous test calculations, we decided to include basis functions with $j \leq 9/2$ and $L \leq 8$, which gives convergence of the cross sections to within approximately 1%.

4.2 Results

The lowest rotational state of OH in its ground $X^2\Pi$ state at zero field is a Λ doublet with $j = 3/2$. The doublet consists of two states, referred to as e and f, which have opposite parity and are separated by 0.059 cm^{-1}, with $|j = 3/2, e\rangle$ being the ground state. A magnetic field splits each component of the doublet into four states differing by the projection of the angular momentum m_j on the field axis ($m_j = 3/2, 1/2, -1/2, -3/2$). For the N atom in its ^{4}S ground state, a magnetic field produces four Zeeman levels, with spin projections $m_{s_1} = 3/2$, 1/2, $-1/2$ and $-3/2$. The combination of 8 Zeeman levels of OH with 4 of the N atom yields 32 asymptotic levels (thresholds), as shown in Fig. 2. In principle, even at zero field each of the levels is further split due to hyperfine interactions, although in the present work hyperfine effects are neglected for simplicity.

N and OH can both be magnetically trapped in their spin-stretched states, with $m_{s_1} = 3/2$ and $m_j = 3/2$, respectively. There are two such states for OH, originating from the e and f components of the Λ doublet. We choose the initial state to be $|m_{s_1} = 3/2\rangle|m_j = 3/2, e\rangle$, shown with a red line in Fig. 2. This is likely to be more favourable for sympathetic cooling than $|m_{s_1} = 3/2\rangle|m_j = 3/2, f\rangle$ (shown with a solid blue line in Fig. 2), because there are fewer inelastic channels open for Zeeman relaxation at low collision energies. In particular, we avoid transitions between the two fully spin-stretched states, from $|m_{s_1} = 3/2\rangle|m_j = 3/2, f\rangle$ to $|m_{s_1} = 3/2\rangle|m_j = 3/2, e\rangle$, at collision energies below about 85 mK. The only centrifugal suppression in such a process, even for an incoming s wave ($L_i = 0, M_{L,i} = 0$) is due to a p-wave barrier in the outgoing channel ($L_f = 1, M_{L,f} = 0$) with a height of only 11 mK, necessitated by the change in OH monomer parity.

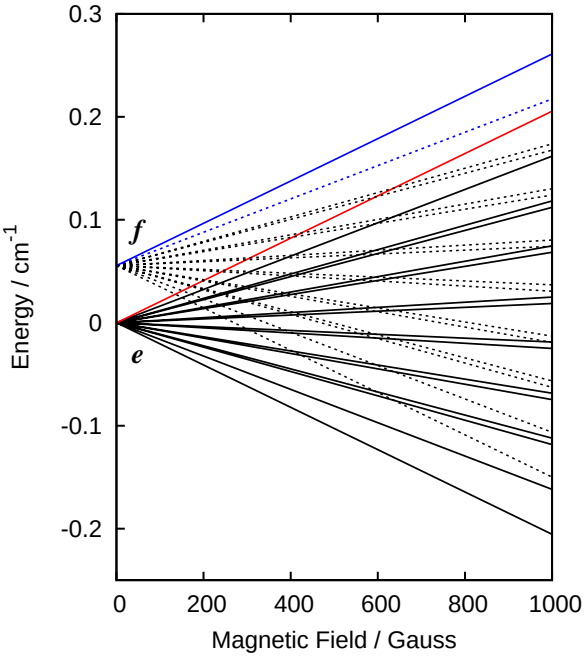

Fig. 2 Energy levels of noninteracting N(^{4}S)+OH($X^2\Pi, j = 3/2$) in a magnetic field. The solid red and blue lines indicates the spin-stretched low-field-seeking states $|m_{s_1} = 3/2\rangle|m_j = 3/2, e\rangle$ (red) and $|m_{s_1} = 3/2\rangle|m_j = 3/2, f\rangle$ (blue). The dotted blue line shows state $|m_{s_1} = 3/2\rangle|m_j = 1/2, f\rangle$.

The interaction between collision partners that are initially in fully spin-stretched states takes place almost entirely on the quintet (high-spin) potential energy surfaces. A full description of exit channels in which $m_{s_1} + m_j$ has changed requires triplet surfaces, but including these explicitly would be computationally prohibitively expensive. In the present work, we effectively approximate the triplet potential surfaces with the corresponding quintet ones. This approximation is closely analogous to that used for N+NH in ref.[44].

In a low-energy inelastic collision, the quantum state of at least one of the colliding species changes and kinetic energy is released. There are two main mechanisms that produce inelasticity in ultracold collisions of an open-shell S-state atom with a molecule in a $^2\Pi$ state. The first is direct coupling through the anisotropy of the interaction potential, which drives transitions to states with the molecular quantum number m_j reduced by at least 1 and the atomic spin projection m_{s_1} unchanged. This mechanism is also present in col-

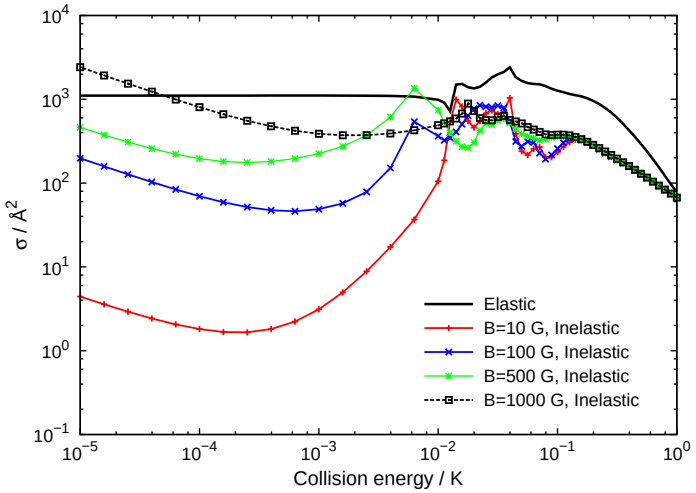

Fig. 3 Elastic and total inelastic cross sections for N+OH scattering at different magnetic field strengths B. The elastic cross section is almost unaffected by the field strength and is shown only for $B = 10$ G.

lisions between a closed-shell atom and a $^2\Pi$ molecule and has been described by Tscherbul *et al.*[33]. The second mechanism arises from coupling by the spin-spin dipolar interaction $\hat{H}_{s_1s_2}$. Here, the final Zeeman state may have quantum numbers m_j and m_{s_1} reduced by at most one. Such processes are also present in collisions of an open-shell S-state atom with $^2\Sigma$ or $^3\Sigma$ molecules, or indeed between two alkali-metal atoms. Collisions of spin-polarized S-state atoms with $^2\Pi$ molecules thus combine two direct mechanisms for coupling between different Zeeman levels.

The most important contribution to coupling by the interaction potential comes from the anisotropic term $V_{20}(R)$, which induces direct transitions from the OH state $|m_j = 3/2, e\rangle$ to $|m_j = 1/2, e\rangle$ and $|m_j = -1/2, e\rangle$. This occurs even in the s-wave regime ($L_i = 0$). An s-wave collision in which $m_{s_1} + m_j$ decreases requires $M_{L,f} > 1$ to conserve $M_{\rm tot}$. If the monomer parity is unchanged, conservation of total parity then requires $L_f \geq 2$. There is thus a centrifugal barrier in the outgoing channel, which suppresses the inelastic cross sections for low collision energies and low fields. For N+OH, the centrifugal barriers are relatively high due to the low reduced mass and small C_6^{00} coefficient: the height of the d-wave barrier is 71 mK.

Fig. 3 shows the cross sections for Zeeman relaxation in collisions of OH($X^2\Pi, |m_j = 3/2, e\rangle$) with N(^{4}S, $|m_{s_1} = 3/2\rangle$) for magnetic field strengths $B = 10$, 100, 500 and 1000 G. At low collision energies (below 0.1 mK), the cross sections behave according to the Wigner threshold laws[64]: the elastic cross section is constant, while the total inelastic cross section grows with decreasing energy as $E^{-1/2}$. The elastic cross section is almost unaffected by the magnetic field. At ultralow collision energies, the inelastic cross sections are suppressed due to centrifugal barriers in the outgoing channels, and the total inelastic cross section grows with increasing field because the increasing kinetic energy release helps overcome these barriers. For example, the energy released by relaxation to the state $|m_{s_1} = 3/2\rangle|m_j = -1/2, e\rangle$ at a field of 560 G is sufficient to overcome the d-wave barrier, and Fig. 3 shows how the inelastic cross section is enhanced for fields of 500 G and higher in the s-wave regime. For collision energies between 4 mK and 80 mK, both the elastic and inelastic cross sections feature numerous resonances, mostly Feshbach resonances due to coupling with higher-energy closed channels.

As discussed above, there are two mechanisms driving transitions between different Zeeman levels, one driven by the spin-spin dipolar term $\hat{H}_{s_1s_2}$ and the other driven by the anisotropy of the intermolecular potential $V_{kq}(R)$. The mechanism involving $\hat{H}_{s_1s_2}$ dominates for low fields (10 G and below) and in the s-wave regime. For higher fields (100 G and

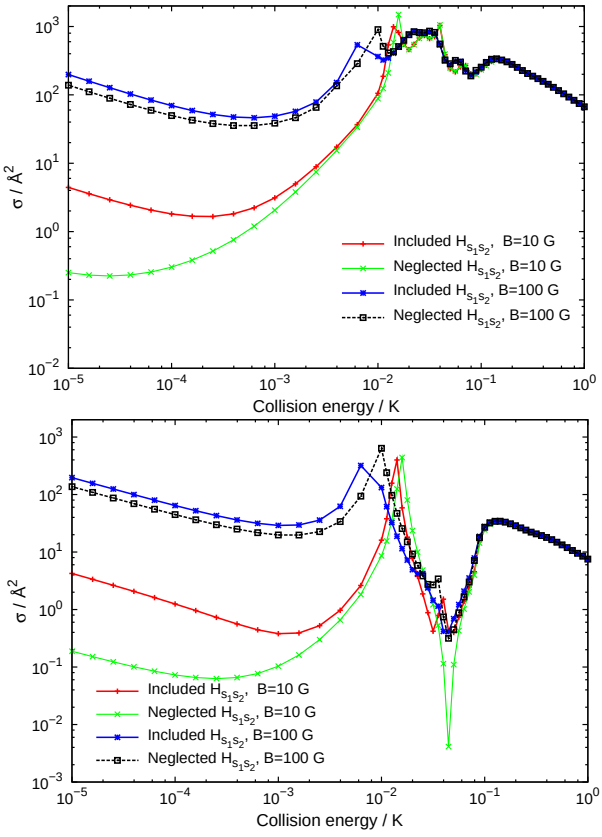

Fig. 4 Comparison of the total inelastic cross sections (upper panel) and the s-wave contributions to them (lower panel) for N+OH, obtained with the spin-spin dipolar interaction included or neglected in the Hamiltonian, for magnetic fields $B = 10$ and 100 G.

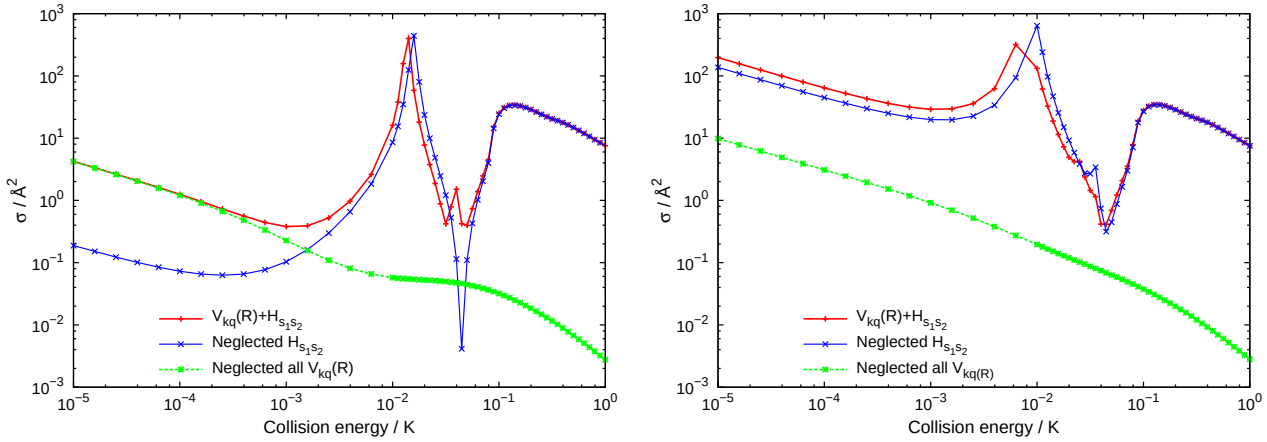

Fig. 5 Comparison of the s wave total inelastic cross sections for N+OH with those obtained with either the spin-spin dipolar term or the anisotropy of the interaction potential neglected. Left-hand panel: $B = 10$ G; right-hand panel: $B = 100$ G.

above), the opposite is true and the relaxation is driven by $V_{kq}(R)$. Fig. 4 shows the integral cross sections and the s-wave contribution for the two lowest fields (10 and 100 G), with the $\hat{H}_{\mathrm{s_1s_2}}$ term in the Hamiltonian included or neglected. Fig. 5 compares the s-wave contributions for the same two fields with those obtained by neglecting either the spin-spin dipolar term $\hat{H}_{\mathrm{s_1s_2}}$ or all the anisotropic terms $V_{kq}(R)$. At 10 G, $\hat{H}_{\mathrm{s_1s_2}}$ greatly enhances inelastic processes in the ultracold regime: at 10^{-5} K, the enhancement is almost two orders of magnitude. However, for $B = 100$ G, $V_{kq}(R)$ is dominant over the whole range of energies.

The way in which the spin-spin dipolar interaction induces transitions between different Zeeman levels is exactly parallel to that described by Janssen *et al.*[65,66]. It is a purely long-range effect caused by narrowly avoided crossings between the potential adiabats at very long range, which enable transitions between Zeeman levels without the need to penetrate centrifugal barriers. In the present case, avoided crossings due to the dipolar term are present between the adiabat asymptotically correlating with the incident s-wave channel $|m_{s_1} = 3/2\rangle|m_j = 3/2, e\rangle$ and other adiabats correlating with the states $|m_{s_1} = 3/2\rangle|m_j = 1/2, e\rangle$, $|m_{s_1} = 1/2\rangle|m_j = 3/2, e\rangle$, and $|m_{s_1} = 1/2\rangle|m_j = 1/2, e\rangle$. The p-wave and higher-L contributions to the total inelastic cross sections are almost unaffected by the inclusion of $\hat{H}_{\mathrm{s_1s_2}}$ for any field and collision energy. This arises because the long-range avoided crossings for incident channels with centrifugal barriers are energetically inaccessible at low energies.

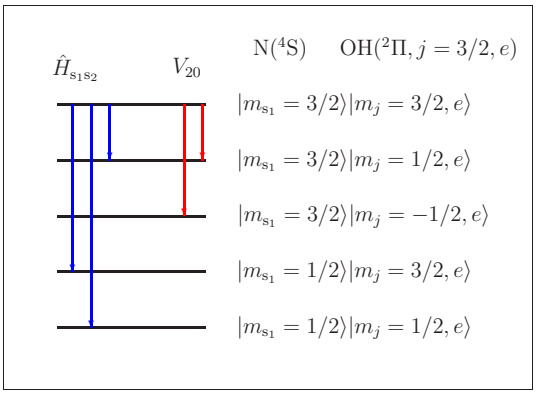

Fig. 6 Pattern of first-order couplings between different Zeeman levels of N(^{4}S)+OH($X^2\Pi, j = 3/2$) through the spin-spin dipolar interaction and the anisotropy of the interaction potential, for incoming s wave ($L_i = 0$) and outgoing d wave ($L_f = 2$).

Channels corresponding to different Zeeman levels are also directly coupled by the anisotropy of the intermolecular potential $V_{kq}(R)$. Fig. 6 shows a schematic illustration of the first-order couplings by $\hat{H}_{\mathrm{s_1s_2}}$ and $V_{kq}(R)$ for collisions involving an incoming s wave and outgoing d waves. Because of this, long-range avoided crossings are present even if we neglect $\hat{H}_{\mathrm{s_1s_2}}$. However, the effect of the avoided crossings on collision outcomes is much more pronounced for crossings due to $\hat{H}_{\mathrm{s_1s_2}}$ than for those due to $V_{kq}(R)$. The latter dies off much faster with R than $\hat{H}_{\mathrm{s_1s_2}}$, and is one or two orders of magnitude weaker at the positions of the long-range avoided crossings. The ratio of the coupling strengths is approximately $\hat{H}_{\mathrm{s_1s_2}}(R)/V_{20}(R) = E_{\mathrm{h}}\alpha^2/C_6^{20}(R/a_0)^{-3}$. The avoided crossings for $B = 10$ G occur at distances ranging from 159 to 342 a_0, corresponding to a ratio $\hat{H}_{\mathrm{s_1s_2}}(R)/V_{20}(R)$ between 10 and 100. It follows from an approximate Landau-Zener model[67] that the probability of ending in a different asymptotic level after a nonadiabatic transition is proportional to the square of the coupling between the diabats if the coupling is relatively small.

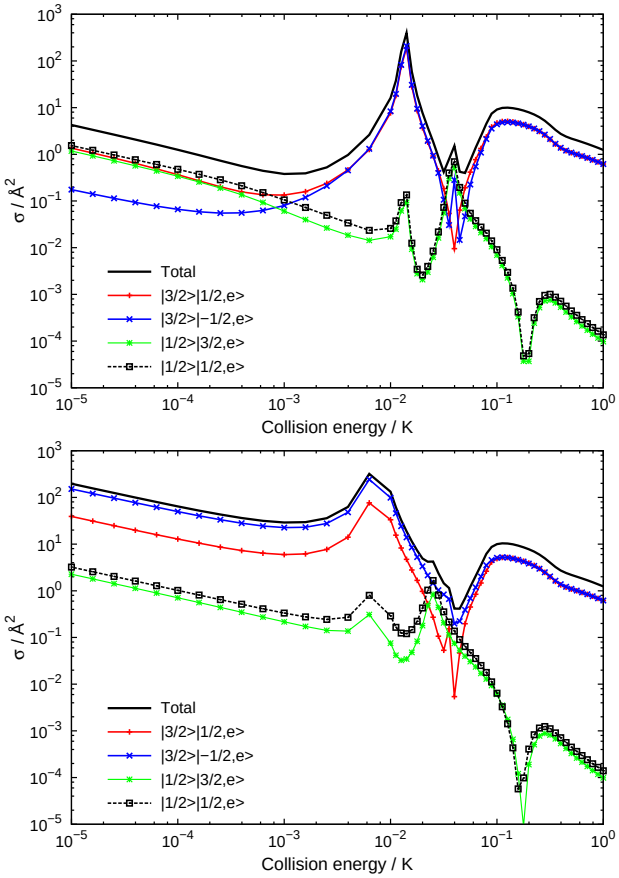

Fig. 7 State-to-state inelastic cross sections (s-wave contribution only) for fields of 10 G (upper panel) and 100 G (lower panel).

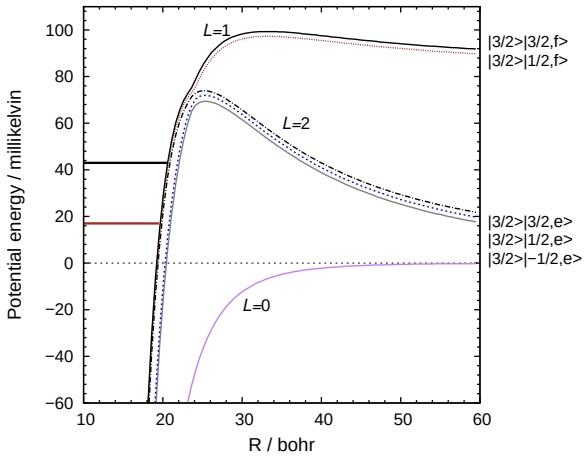

Fig. 8 The lowest adiabatic potential energy curves for $M_{\rm tot} = 3$ and $L_{\rm max} = 2$ correlating with thresholds with the state of the N atom unchanged ($|m_{s_1} = 3/2\rangle$), at $B = 10$ G. Two solid horizontal lines indicates the position of the bound states responsible for the two sharp Feshbach resonances in the s and d-wave contribution to the inelastic cross sections.

The interplay between the spin-spin dipolar term and the intermolecular potential terms is also manifested in the state-to-state cross sections. Fig. 7 shows state-to-state cross sections (s-wave contributions only) for $B = 10$ G and 100 G. At $B = 10$ G, in the region where the $\hat{H}_{\rm s_1 s_2}$ term dominates (below 1 mK), the most important transitions are to states with m_j or m_{s_1} quantum numbers reduced by 1, which are those coupled to the incident channel $|m_{s_1} = 3/2\rangle|m_j = 3/2, e\rangle$ by $\hat{H}_{\rm s_1 s_2}$, while for collision energies above 1 mK the dominant inelastic channels become $|m_{s_1} = 3/2\rangle|m_j = 1/2, e\rangle$ and $|m_{s_1} = 3/2\rangle|m_j = -1/2, e\rangle$, which are those coupled by $V_{kq}(R)$. At $B = 100$ G, only channels coupled by $V_{kq}(R)$ are important.

The s-wave cross sections at $B = 10$ G exhibit two distinct resonant structures: a strong feature near 15 mK and a weaker one around 41 mK. Both are Feshbach resonances caused by coupling to closed channels arising from the f component of the Λ doublet of OH. The coupling arises almost exclusively from the $V_{10}(R)$ term in the intermolecular potential, which couples states of different monomer parity. The Feshbach resonance near 15 mK can be attributed to a bound state on the p-wave adiabat correlating with the $|m_{s_1} = 3/2\rangle|m_j = 1/2, f\rangle$ threshold, as shown in Fig. 8. This resonance moves to smaller energies with increasing field, because the energy difference between the $|m_j = 3/2, e\rangle$ and $|m_j = 1/2, f\rangle$ states (red and dotted blue lines in Fig. 2, respectively) decreases as the field increases. For sufficiently large field ($B > 1200$ G), this resonance will disappear as the $|m_j = 1/2, f\rangle$ level drops below $|m_j = 3/2, e\rangle$. The second Feshbach resonance near 41 mK can be attributed to a bound state on the p-wave adiabat correlating with the $|m_{s_1} = 3/2\rangle|m_j = 3/2, f\rangle$ threshold. The position of this resonance is almost unaffected by the field strength since the energy difference between the two spin-stretched states, $|m_j = 3/2, e\rangle$ and $|m_j = 3/2, f\rangle$, is independent of magnetic field.

The fact that these are Feshbach (rather than shape) resonances is confirmed by several observations. First, the d-wave contributions to the inelastic cross sections show resonant structures at exactly the same energies as the s-wave contribution. Secondly, the positions and shapes of the Feshbach resonances can be reproduced using even the smallest possible basis set that allows inelastic transitions, with $j \leq 3/2$, $L \leq 2$, and potential terms $V_{kq}(R)$, $k \leq 2$. Thirdly, the presence of the $V_{10}(R)$ term, which does not couple the incident and outgoing channels directly, is crucial for the existence of the resonances. It is worth noting that no such structure due to Feshbach resonances would be present for collisions involving the initial state $|m_{s_1} = 3/2\rangle|m_j = 3/2, f\rangle$, with OH in the upper component of its Λ doublet, since no low-lying closed channels are present in that case. However, molecules in the

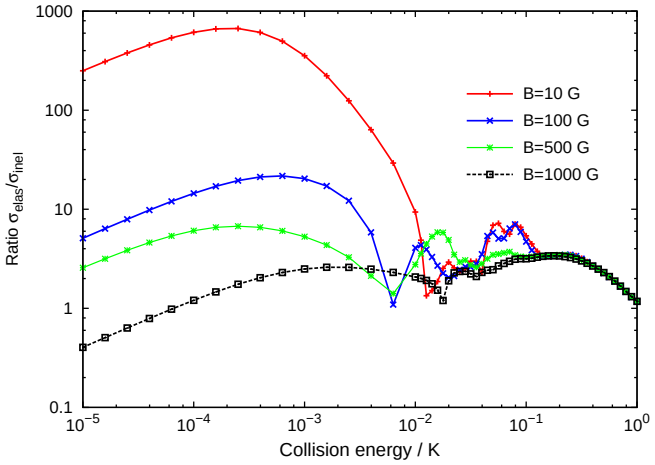

Fig. 9 Ratio of elastic to total inelastic cross sections for N+OH at different magnetic fields.

f state are likely to undergo fast relaxation to the e state in collisions driven directly by $V_{10}(R)$.

Fig. 9 shows the ratio of the elastic to total inelastic cross sections as a function of collision energy. The ratio is not favourable for sympathetic cooling of OH by collision with ultracold N atoms, except at fields below 10 G and collision energies below 1 mK. The cross sections presented here may be compared to those for N(^{4}S)+NH($^3\Sigma^-$) by Żuchowski and Hutson[44]. The ratio of the elastic to inelastic cross sections is at least an order of magnitude lower for N+OH than for N+NH. Two main reasons for this can be identified. First, the spin-stretched component of the rotational ground state of NH ($^3\Sigma^-$, $n = 0$) is not directly coupled by the potential anisotropy to any other accessible Zeeman level, whereas such a coupling does exist for the ground state of OH($^2\Pi, j = 3/2$) (or any other molecule with $j \geq 1$). Secondly, there are low-lying states arising from the f component of the Λ doublet in the OH radical that create many Feshbach resonances and increase the inelasticity. Both effects are particularly strong for collision energies above 10 mK, where the contributions from p and d incoming waves to the inelastic cross sections are dominant. For all field strengths, the ratio of elastic to inelastic cross sections at collision energies above 1 mK is more than 10 times larger for N+NH than for N+OH.

4.3 Potential dependence

The results of scattering calculations at ultralow collision energies are in general very sensitive to the details of interaction potentials. To estimate the accuracy of the calculated potential energy surfaces for N+OH, we have carried out additional electronic structure calculations for the geometry corresponding to the global minimum of the potentials at the linear N–OH geometry. In the aug-cc-pV5Z basis set, the global minimum has a well depth of 120.9 cm^{-1}, while in the aug-cc-pV6Z basis set this shifts to 121.8 cm^{-1}. Based on these two results, we can estimate the complete basis set limit of the CCSD(T) method to be 122.9 cm^{-1}, using the extrapolation formula for correlation energy as given in Ref.[68]. This corresponds to an error estimate of 1.7% for our full potential surfaces using the aug-cc-pV5Z basis set. To estimate the error in the correlation energy obtained from the CCSD(T) method, we have performed full configuration-interaction (FCI) calculations with eight electrons correlated in the cc-pVDZ basis set. The relative contribution of the FCI correction to the CCSD(T) result should only be weakly dependent on the basis set used, so even in the small cc-pVDZ basis set we should obtain a reliable estimate of the FCI valence-valence correlation correction. The FCI correction to the CCSD(T) result accounts for approximately 1.5% of the interaction energy at the global minimum. We can thus estimate the uncertainty of our potential energy surfaces to be 4% at worst.

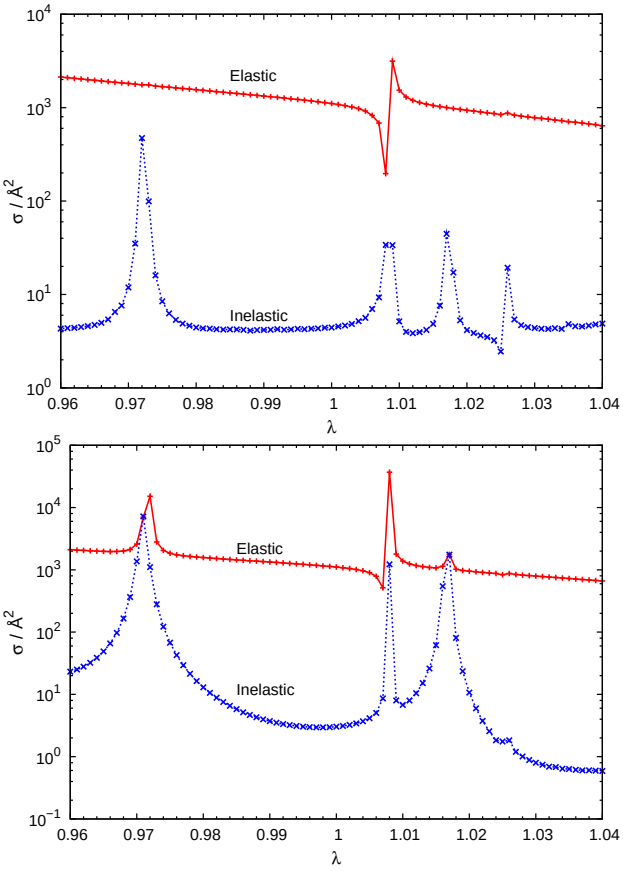

Fig. 10 Cross sections obtained with the interaction potential scaled by a constant factor, $V(R) \rightarrow \lambda \cdot V(R)$, for magnetic field $B = 10$ G and collision energies of 10 μK (upper panel) and 1 mK (lower panel).

To assess the sensitivity of the scattering results to the uncertainty in the interaction potential, we have carried out calculations with the interaction potential scaled by a constant factor λ in the range $0.96 \leq \lambda \leq 1.04$, corresponding to the estimated error bounds in the calculated potential energy surfaces. The results at $B = 10$ G are shown in Fig. 10 for collision energies of 1 mK and 10 μK. The weak dependence of the cross sections on the potential scaling is disturbed by the presence of sharp resonances, which occur when bound states of the N-OH complex cross the incoming threshold (or more precisely the collision energy) as a function of λ. Two of the peaks in the inelastic cross sections, near $\lambda = 1.010$ and $\lambda = 1.026$, can be attributed to the Feshbach resonances in the s and d partial-wave contributions discussed above. The two additional peaks at $\lambda = 0.97$ and $\lambda = 1.017$, which broaden substantially with collision energy, are due to shape resonances in the p-wave partial cross section. If the true potential happens to bring one of these resonances close to zero energy, it may change the ratio of elastic to inelastic cross sections quite dramatically. However, Fig. 10 shows that the resonances occur in quite narrow ranges of λ, so that there is a low probability that the true potential will be such that the ratio of elastic to inelastic cross sections is seriously affected by resonances for collision energies below 1 mK. It may also be noted that the numerical results obtained with the unscaled potential ($\lambda = 1$) are fairly typical of the range expected for N+OH on plausible interaction potentials, in the sense that the low-energy elastic cross section (around 1000 Å^2) is close to the value $\sigma = 4\pi\bar{a}^2 = 712$ Å^2 obtained from the mean scattering length $\bar{a}$ defined by Gribakin and Flambaum[69].

5 Summary and conclusions

We have presented a theoretical study of the relaxation processes in collisions between an atom in an open-shell S state and a molecule in a $^2\Pi$ state, in a magnetic field, using the example of N(^{4}S)+OH($^2\Pi$). The transitions between different Zeeman levels in such collisions are driven by two mechanisms: coupling through the spin-spin dipolar term and through the anisotropy of the interaction potential. Both mechanisms are present in first order. The spin-spin dipolar term dominates when both the collision energy and the magnetic field are low, while the anisotropy of the interaction potential dominates at higher energies or fields. In the latter regime, the spin-spin dipolar term can be neglected. Neglecting the dipolar interaction is equivalent to treating the atom as closed-shell, which dramatically reduces the cost of the scattering calculations.

An important general point is that spin relaxation collisions can be driven directly by the anisotropy of the interaction potential for any molecule that has rotational angular momentum. Since the anisotropies of atom-molecule and molecule-molecule interaction potentials are typically quite large, this will often provide an important trap loss mechanism for such states. For molecules in $^2\Pi$ states, this is true even for the molecular ground state.

For the case of N+OH, the spin-spin dipolar term dominates at collision energies below about 1 mK and magnetic fields of 10 G or less. In this regime, the ratio of elastic to inelastic cross sections is greater than 100 and thus favourable for sympathetic cooling. However, if either the collision energy or the magnetic field is significantly above this, inelastic processes due to the potential anisotropy dominate and the ratio of elastic to inelastic cross sections falls. This suggests that sympathetic cooling of OH by collisions with N atoms is unlikely to be successful except at collision energies below 1 mK.

Acknowledgments

The authors are grateful to the Polish Ministry of Science and Higher Education (project N N204 215539) and to the UK Engineering and Physical Sciences Research Council for financial support. The collaboration was supported by the EuroQUAM Programme of the European Science Foundation.

References

1 M. H. Anderson, J. R. Ensher, M. R. Matthews, C. E. Wieman and E. A. Cornell, *Science*, 1995, **269**, 198–201.
2 E. R. Hudson, H. J. Lewandowski, B. C. Sawyer and J. Ye, *Phys. Rev. Lett.*, 2006, **96**, 143004.
3 M. R. Tarbutt, J. J. Hudson, B. E. Sauer and E. A. Hinds, *Faraday Discuss.*, 2009, **142**, 37–56.
4 S. Tojo, M. Kitagawa, K. Enomoto, Y. Kato, Y. Takasu, M. Kumakura and Y. Takahashi, *Phys. Rev. Lett.*, 2006, **96**, 153201.
5 K. Enomoto, M. Kitagawa, S. Tojo and Y. Takahashi, *Phys. Rev. Lett.*, 2008, **100**, 123001.
6 P. Rabl, D. DeMille, J. M. Doyle, M. D. Lukin, R. J. Schoelkopf and P. Zoller, *Phys. Rev. Lett.*, 2006, **97**, 033003.
7 D. DeMille, *Phys. Rev. Lett.*, 2002, **88**, 067901.
8 R. V. Krems, *Phys. Chem. Chem. Phys.*, 2008, **10**, 4079–4092.
9 J. M. Hutson, *Science*, 2010, **327**, 788–789.
10 S. Ospelkaus, K.-K. Ni, D. Wang, M. H. G. de Miranda, B. Neyenhuis, G. Quéméner, P. S. Julienne, J. L. Bohn, D. S. Jin and J. Ye, *Science*, 2010, **327**, 853–857.
11 C. N. Cohen-Tannoudji, *Rev. Mod. Phys.*, 1998, **70**, 707–719.
12 K.-K. Ni, S. Ospelkaus, M. H. G. de Miranda, A. Pe'er, B. Neyenhuis, J. J. Zirbel, S. Kotochigova, P. S. Julienne, D. S. Jin and J. Ye, *Science*, 2008, **322**, 231–235.
13 J. Deiglmayr, A. Grochola, M. Repp, K. Mörtlbauer, C. Glück, J. Lange, O. Dulieu, R. Wester and M. Weidemüller, *Phys. Rev. Lett.*, 2008, **101**, 133004.
14 J. G. Danzl, M. J. Mark, E. Haller, M. Gustavsson, R. Hart, J. Aldegunde, J. M. Hutson and H.-C. Nägerl, *Nature Phys.*, 2010, **6**, 265–270.
15 P. S. Żuchowski, J. Aldegunde and J. M. Hutson, *Phys. Rev. Lett.*, 2010, **105**, 153201.
16 H. L. Bethlem, G. Berden and G. Meijer, *Phys. Rev. Lett.*, 1999, **83**, 1558–1561.

17 H. L. Bethlem, G. Berden, F. M. H. Crompvoets, R. T. Jongma, A. J. A. van Roij and G. Meijer, *Nature*, 2000, **406**, 491.

18 S. K. Tokunaga, J. M. Dyne, E. A. Hinds and M. R. Tarbutt, *New J. Phys.*, 2009, **11**, 055038.

19 J. J. Gilijamse, S. Hoekstra, S. Y. T. van de Meerakker, G. C. Groenenboom and G. Meijer, *Science*, 2006, **313**, 1617–1620.

20 J. D. Weinstein, R. deCarvalho, T. Guillet, B. Friedrich and J. M. Doyle, *Nature*, 1998, **395**, 148–150.

21 D. J. Larson, J. C. Bergquist, J. J. Bollinger, W. M. Itano and D. J. Wineland, *Phys. Rev. Lett.*, 1986, **57**, 70–73.

22 A. Ostendorf, C. B. Zhang, M. A. Wilson, D. Offenberg, B. Roth and S. Schiller, *Phys. Rev. Lett.*, 2006, **97**, 243005.

23 C. J. Myatt, E. A. Burt, R. W. Ghrist, E. A. Cornell and C. E. Wieman, *Phys. Rev. Lett.*, 1997, **78**, 586–589.

24 G. Modugno, G. Ferrari, G. Roati, R. J. Brecha, A. Simoni and M. Inguscio, *Science*, 2001, **294**, 1320–1322.

25 J. van Veldhoven, H. L. Bethlem and G. Meijer, *Phys. Rev. Lett.*, 2005, **94**, 083001.

26 P. Soldán and J. M. Hutson, *Phys. Rev. Lett.*, 2004, **92**, 163202.

27 A. O. G. Wallis and J. M. Hutson, *Phys. Rev. Lett.*, 2009, **103**, 183201.

28 Tokunaga, S.K., Skomorowski, W., Zuchowski, P.S., Moszynski, R., Hutson, J.M., Hinds, E.A. and Tarbutt, M.R., *Eur. Phys. J. D*, 2011.

29 W. Skomorowski, F. Pawlowski, T. Korona, R. Moszynski, P. S. Żuchowski and J. M. Hutson, *J. Chem. Phys.*, 2011, **134**, 114109.

30 P. S. Żuchowski and J. M. Hutson, *Phys. Rev. A*, 2009, **79**, 062708.

31 T. V. Tscherbul, H.-G. Yu and A. Dalgarno, *Phys. Rev. Lett.*, 2011, **106**, 073201.

32 L. P. Parazzoli, N. J. Fitch, P. S. Żuchowski, J. M. Hutson and H. J. Lewandowski, *Phys. Rev. Lett.*, 2011, **106**, 193201.

33 T. V. Tscherbul, G. C. Groenenboom, R. V. Krems and A. Dalgarno, *Faraday Discuss.*, 2009, **142**, 127–141.

34 Z. Pavlovic, T. V. Tscherbul, H. R. Sadeghpour, G. C. Groenenboom and A. Dalgarno, *J. Phys. Chem. A*, 2009, **113**, 14670–14680.

35 A. V. Avdeenkov and J. L. Bohn, *Phys. Rev. A*, 2002, **66**, 052718.

36 M. Lara, J. L. Bohn, D. E. Potter, P. Soldán and J. M. Hutson, *Phys. Rev. A*, 2007, **75**, 012704.

37 M. H. Alexander, *J. Chem. Phys.*, 1982, **76**, 5974–5988.

38 B. C. Sawyer, B. K. Stuhl, D. Wang, M. Yeo and J. Ye, *Phys. Rev. Lett.*, 2008, **101**, 203203.

39 M. Kirste, L. Scharfenberg, J. Kłos, F. Lique, M. H. Alexander, G. Meijer and S. Y. T. van de Meerakker, *Phys. Rev. A*, 2010, **82**, 042717.

40 L. Scharfenberg, J. Klos, P. J. Dagdigian, M. H. Alexander, G. Meijer and S. Y. T. van de Meerakker, *Phys. Chem. Chem. Phys.*, 2010, **12**, 10660–10670.

41 L. Scharfenberg, S. Y. T. van de Meerakker and G. Meijer, *Phys. Chem. Chem. Phys.*, 2011.

42 S. Y. T. van de Meerakker and G. Meijer, *Faraday Discuss.*, 2009, **142**, 113–126.

43 T. V. Tscherbul, J. Kłos, A. Dalgarno, B. Zygelman, Z. Pavlovic, M. T. Hummon, H.-I. Lu, E. Tsikata and J. M. Doyle, *Phys. Rev. A*, 2010, **82**, 042718.

44 P. S. Żuchowski and J. M. Hutson, *Phys. Chem. Chem. Phys.*, 2011, **13**, 3669–3680.

45 M. T. Hummon, T. V. Tscherbul, J. Kłos, H.-I. Lu, E. Tsikata, W. C. Campbell, A. Dalgarno and J. M. Doyle, *Phys. Rev. Lett.*, 2011, **106**, 053201.

46 F. Pauzat, Y. Ellinger, G. Berthier, M. Grin and Y. Viala, *Chem. Phys.*, 1993, **174**, 71 – 79.

47 D. Sengupta and A. K. Chandra, *J. Chem. Phys.*, 1994, **101**, 3906–3915.

48 R. Guadagnini, G. C. Schatz and S. P. Walch, *J. Chem. Phys.*, 1995, **102**, 774–783.

49 R. Guadagnini, G. C. Schatz and S. P. Walch, *J. Chem. Phys.*, 1995, **102**, 784–791.

50 M. Jorfi, P. Honvault and P. Halvick, *J. Chem. Phys.*, 2009, **131**, 094302.

51 D. Edvardsson, C. F. Williams and D. C. Clary, *Chem. Phys. Lett.*, 2006, **431**, 261 – 266.

52 L. M. C. Janssen, G. C. Groenenboom, A. van der Avoird, P. S. Żuchowski and R. Podeszwa, *J. Chem. Phys.*, 2009, **131**, 224314.

53 T. H. Dunning, Jr., *J. Chem. Phys.*, 1989, **90**, 1007–1023.

54 S. F. Boys and F. Bernardi, *Mol. Phys.*, 1970, **19**, 553.

55 H.-J. Werner, P. J. Knowles, F. R. M. R. Lindh, M. Schütz, P. Celani, T. Korona, A. Mitrushenkov, G. Rauhut, T. B. Adler, R. D. Amos, A. Bernhardsson, A. Berning, D. L. Cooper, M. J. O. Deegan, A. J. Dobbyn, E. G. F. Eckert, C. Hampel, G. Hetzer, T. Hrenar, G. Knizia, C. Köppl, Y. Liu, A. W. Lloyd, R. A. Mata, A. J. May, S. J. McNicholas, W. Meyer, M. E. Mura, A. Nicklass, P. Palmieri, K. Pflüger, R. Pitzer, M. Reiher, U. Schumann, H. Stoll, A. J. Stone, R. Tarroni, T. Thorsteinsson, M. Wang and A. Wolf, *MOLPRO, version 2008.1, a package of ab initio programs*, 2008.

56 G. C. Nielson, G. A. Parker and R. T Pack, *J. Chem. Phys.*, 1976, **64**, 2055–2061.

57 W. Skomorowski and R. Moszynski, *J. Chem. Phys.*, 2011, **134**, 124117.

58 T.-S. Ho and H. Rabitz, *J. Chem. Phys.*, 1996, **104**, 2584–2597.

59 J. M. Brown and A. Carrington, *Rotational Spectroscopy of Diatomic Molecules*, Cambridge University Press, Cambridge, U.K., 2003.

60 J. M. Hutson and S. Green, *MOLSCAT computer program, version 14, distributed by Collaborative Computational Project No. 6 of the UK Engineering and Physical Sciences Research Council*, 2006.

61 M. H. Alexander and D. E. Manolopoulos, *J. Chem. Phys.*, 1987, **86**, 2044–2050.

62 C. Ticknor and J. L. Bohn, *Phys. Rev. A*, 2005, **71**, 022709.

63 J. M. Brown, K. Kaise, C. M. L. Kerr and D. J. Milton, *Mol. Phys.*, 1978, **36**, 553.

64 E. P. Wigner, *Phys. Rev.*, 1948, **73**, 1002–1009.

65 L. M. C. Janssen, P. S. Żuchowski, A. van der Avoird, G. C. Groenenboom and J. M. Hutson, *Phys. Rev. A*, 2011, **83**, 022713.

66 Janssen, L.M.C., van der Avoird, A. and Groenenboom, G.C., *Eur. Phys. J. D*, 2011.

67 E. E. Nikitin, in *Handbook of Atomic, Molecular and Optical Physics*, ed. G. W. F. Drake, Springer Science+Business Media, New York, USA, 2006, pp. 741–752.

68 K. L. Bak, A. Halkier, P. Jørgensen, J. Olsen, T. Helgaker and W. Klopper, *J. Mol. Struct.*, 2001, **567**, 375–384.

69 G. F. Gribakin and V. V. Flambaum, *Phys. Rev. A*, 1993, **48**, 546.